Two mathematical models of five-phase high speed permanent magnet bearingless slice motor

Tuocheng NI[a], Xiaolin WANG[a], Qiang DING[a],Guyu WU[a]

[a]Nanjing University of Aeronautics and Astronautics, Yudao street 29, 20016 Nanjing, China, wangxl@nuaa.edu.cn

Abstract—Most bearingless motors run at a relatively low speed because of the high iron loss problem. Considering that a slotless structure is beneficial to high speed, this paper deduces two mathematical models based on this existent structure. The first model is for traditional control and the second one is for fault-tolerant control. In the process of derivation, the concept of superposition is introduced to calculate the flux density in the air gap. At last, finite element analysis is done to verify the model.

Keywords-mathematical models, permanent magnet bearingless slice motor (PMBSM), slotless structure, fault-tolerant

I. INTRODUCTION

Due to its simple and compact structure, the permanent magnet bearingless slice motor (PMBSM) has been used in various industry fields such as hazardous chemical material process, blood pumps for artificial heart assistance device and ultra-pure fluid pumps in semiconductor industry[1]. However, these applications mainly focus on low speed field. In [2], a five-phase PMBSM with slotless stator structure is presented for verification of high speed capability about PMBSM, as shown in Fig.1. In [3], winding configuration, loss analysis as well as control system implementation are reported. Nevertheless, the mathematical model of radial levitation force is not given by the authors. It is well known that the mathematical model of radial levitation force is the foundation of control strategy and control system design[4], thus this paper is to establish two kinds of mathematical levitation force models, the first one is for traditional high speed field and the second one is for high reliability application where the PMBSM must possess fault-tolerant capability[5][6]. All of these two mathematical models are deduced from the distribution of air gap magnetic flux density and verified by finite element method.

II. MATHEMATICAL MODEL OF RADIAL LEVITATION FORCE AND TORQUE

We refer the slotless structure in [3] and deduce the mathematical model. Fig.1 shows the structure of this kind of bearingless motor. Two coils of each phase reverse series. The rotor is made up of rotor core and the permanent magnet (PM) . In order to reduce the complexity, the PM has only a pair of poles. To simplify the analysis, a few assumptions are made as follows:

a. Ignore the magnetic saturation and leakage flux;
b. Conductors of windings are evenly distributed along stator circumference;
c. Ignore magnetic motive force drop in iron.

A. Five-Phase Constraint Model

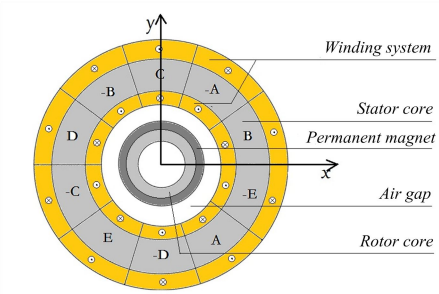

Figure 1. The slotless topology of the bearingless motor

According to working principle of PMBSM, the current in each phase can be spilt into two components, which are called torque current component I_t and levitation current component I_s. Torque current generates one pole-pair magnetic field for drive generation and levitation current generates two pole-pairs magnetic field for levitation force generation. Both of the two components satisfy five-phase constraint relationship, which is described as equation (1).

$$i_k = I_t \cos[\theta_t - \frac{2(k-1)\pi}{5}] + I_s \cos[\theta_t - \frac{4(k-1)\pi}{5}] \quad (1)$$

Where i_k (k=1,2,3,4,5) is the current in each phase. We know that magnetic motive force (MMF) changes linearly under each coil. Change of MMF is directly proportional to the value of the current.

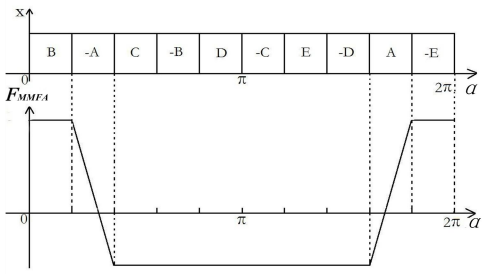

Figure 2. Schematic diagram of magnetic motive force generated by A phase

Take phase-A for example, its distribution of magnetic motive force can be shown in Fig.2 and be expressed as equation (2):

$$F_{MMFA}=\begin{cases}\frac{7\pi}{50}\cdot N_c i_1 \quad 0\le\alpha\le\frac{\pi}{5}\\ (-\alpha+\frac{17\pi}{50})\cdot N_c i_1 \quad \frac{\pi}{5}\le\alpha\le\frac{2\pi}{5}\\ -\frac{3\pi}{50}\cdot N_c i_1 \quad \frac{2\pi}{5}\le\alpha\le\frac{8\pi}{5}\\ (\alpha-\frac{83\pi}{50})\cdot N_c i_1 \quad \frac{8\pi}{5}\le\alpha\le\frac{9\pi}{5}\\ \frac{7\pi}{50}\cdot N_c i_1 \quad \frac{9\pi}{5}\le\alpha\le 2\pi\end{cases} \tag{2}$$

Therefore, the expressions of the MMF generated by all five phases are in the form of piecewise function:

$$F_{MMF}=\begin{cases}[\frac{7\pi}{50}i_1+(\alpha-\frac{3\pi}{50})i_2-\frac{3\pi}{50}i_3-\frac{3\pi}{50}i_4-\frac{3\pi}{50}i_5]N_c \quad 0\le\alpha\le\frac{\pi}{5}\\ [(-\alpha+\frac{17\pi}{50})i_1+\frac{7\pi}{50}i_2-\frac{3\pi}{50}i_3-\frac{3\pi}{50}i_4-\frac{3\pi}{50}i_5]N_c \quad \frac{\pi}{5}\le\alpha\le\frac{2\pi}{5}\\ [-\frac{3\pi}{50}i_1+\frac{7\pi}{50}i_2+(\alpha-\frac{23\pi}{50})i_3-\frac{3\pi}{50}i_4-\frac{3\pi}{50}i_5]N_c \quad \frac{2\pi}{5}\le\alpha\le\frac{3\pi}{5}\\ [-\frac{3\pi}{50}i_1+(-\alpha+\frac{37\pi}{50})i_2+\frac{7\pi}{50}i_3-\frac{3\pi}{50}i_4-\frac{3\pi}{50}i_5]N_c \quad \frac{3\pi}{5}\le\alpha\le\frac{4\pi}{5}\\ [-\frac{3\pi}{50}i_1-\frac{3\pi}{50}i_2+\frac{7\pi}{50}i_3+(\alpha-\frac{43\pi}{50})i_4-\frac{3\pi}{50}i_5]N_c \quad \frac{4\pi}{5}\le\alpha\le\pi\\ [-\frac{3\pi}{50}i_1-\frac{3\pi}{50}i_2+(-\alpha+\frac{57\pi}{50})i_3+\frac{7\pi}{50}i_4-\frac{3\pi}{50}i_5]N_c \quad \pi\le\alpha\le\frac{6\pi}{5}\\ [-\frac{3\pi}{50}i_1-\frac{3\pi}{50}i_2-\frac{3\pi}{50}i_3+\frac{7\pi}{50}i_4+(\alpha-\frac{63\pi}{50})i_5]N_c \quad \frac{6\pi}{5}\le\alpha\le\frac{7\pi}{5}\\ [-\frac{3\pi}{50}i_1-\frac{3\pi}{50}i_2-\frac{3\pi}{50}i_3+(-\alpha+\frac{77\pi}{50})i_4+\frac{7\pi}{50}i_5]N_c \quad \frac{7\pi}{5}\le\alpha\le\frac{8\pi}{5}\\ [(\alpha-\frac{83\pi}{50})i_1-\frac{3\pi}{50}i_2-\frac{3\pi}{50}i_3-\frac{3\pi}{50}i_4+\frac{7\pi}{50}i_5]N_c \quad \frac{8\pi}{5}\le\alpha\le\frac{9\pi}{5}\\ [\frac{7\pi}{50}i_1+\frac{3\pi}{50}i_2-\frac{3\pi}{50}i_3-\frac{3\pi}{50}i_4+(-\alpha+\frac{97\pi}{50})i_5]N_c \quad \frac{9\pi}{5}\le\alpha\le 2\pi\end{cases} \tag{3}$$

Put the torque current component and levitation current component into (3) and we'll get the expressions of MMF distribution generated by these two current components respectively. Plot them and they'll be as shown in Fig.3 and Fig.4.

Fig.3 shows that the torque magnetic motive force distribution along air gap circumference when phase angle of torque current component (θ_t) equals to zero.

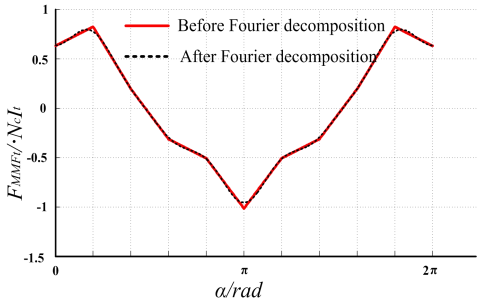

Figure 3. Torque magnet motive force distribution when θ_t=0

Fig.4 shows that the levitation magnetic motive force distribution along air gap circumference when phase angle of levitation current component (θ_s) equals to zero.

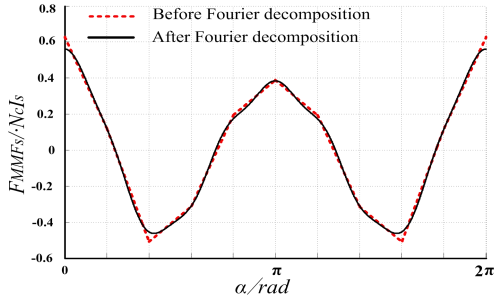

Figure 4. Levitation magnet motive force distribution when θ_s=0

Considering the MMF of air gap is a piecewise function, thus Fourier decomposition is used to obtain a unified expression. It can be seen from Fig.3 and Fig.4 that the fitting curves has good agreement with original curves. Due to the MMF has a linear relationship with flux dentisy when neglecting the rotor eccentricity and the magnetic saturation, the expressions of air gap flux density caused by torque current component and levitation current component can be shown as follows:

$$B_t(\alpha)|_{\theta_t=0}=[a_1\cos\alpha+a_2\cos 4\alpha+a_3\cos 6\alpha]N_c I_t G_\mu \tag{4}$$

$$B_s(\alpha)|_{\theta_s=0}=[a_4\cos 2\alpha+a_5\cos 3\alpha+a_6\cos 8\alpha]N_c I_s G_\mu \tag{5}$$

Where a_i (i=1,2...6) is Fourier decomposition coefficient; N_c is the number of winding conductor in unit radian; G_μ is air gap permeance.

Because the equation (4) and (5) are established at two special positions (θ_t =0 and θ_s =0), the expressions of air gap flux density at general positions can be expressed as:

$$\begin{aligned}B_t(\theta_t,\alpha)=&[a_1\cos(\alpha-\theta_t)+a_2\cos(4\alpha+\theta_t)\\&+a_3\cos(6\alpha-\theta_t)]N_c I_t G_\mu\end{aligned} \tag{6}$$

$$\begin{aligned}B_s(\theta_s,\alpha)=&[a_4\cos(2\alpha-\theta_s)+a_5\cos(3\alpha+\theta_s)\\&+a_6\cos(8\alpha+\theta_s)]N_c I_s G_\mu\end{aligned} \tag{7}$$

According to the Maxwell force formula, the radial forces can be deduced and decomposed into x and y directions:

$$\begin{cases}F_{Mx}=\dfrac{rh}{2\mu_0}\displaystyle\int_0^{2\pi}(B_t+B_s+B_{PM})^2\cos\alpha d\alpha\\ F_{My}=\dfrac{rh}{2\mu_0}\displaystyle\int_0^{2\pi}(B_t+B_s+B_{PM})^2\sin\alpha d\alpha\end{cases} \tag{8}$$

Where B_{PM} is flux density caused by rotor permanent magnets. The torque T can be obtained by virtual work method:

$$T=\frac{dE_g}{d\theta_r}=\frac{d}{d\theta_r}\int_0^{2\pi}\frac{(B_t+B_s+B_{PM})^2 l_m rh}{2\mu_0}d\alpha \tag{9}$$

Where E_g and θ_r stand for the stored energy of air gap and the rotor rotation angle; l_m is equivalent air gap length; r is the radius of rotor; h is the effective axial length. The model can be shown as:

$$\begin{aligned}F_{Mx}=\frac{N_c I_s h\pi r\mu_0}{2l_m^{\,2}}&[a_4a_5N_c I_s\cos 2\theta_s+(a_1a_4+a_2a_5)N_c I_t\cos(\theta_s-\theta_t)\\&+a_4\cos(\theta_s-\theta_r)A_{PM}]\end{aligned} \tag{10}$$

$$F_{My}=\frac{N_c I_s h\pi r\mu_0}{2l_m^{\,2}}[-a_4a_5A_f I_s\sin 2\theta_s+(a_1a_4+a_2a_5)N_c I_t\sin(\theta_s-\theta_t)+a_4\sin(\theta_s-\theta_r)A_{PM}] \quad (11)$$

$$T=\frac{a_1N_c h\pi r\mu_0 A_{PM}}{l_m}I_t\sin(\theta_t-\theta_r) \quad (12)$$

Where A_{PM} denotes the amplitude of magnetic motive force produced by permanent magnet. Considering that in (10) and (11), the values of first two terms are much smaller than the third one which is relevant to the PM magnetic motive. We neglect the first two terms and the model is simplified as:

$$\begin{cases} F_{Mx}=K_M\cos(\theta_s-\theta_r)I_s \\ F_{My}=K_M\sin(\theta_s-\theta_r)I_s \\ T=K_t\sin(\theta_t-\theta_r)I_t \end{cases} \quad (13)$$

Where K_M and K_t are only relevant to the structure of the motor and their values are:

$$\begin{cases} K_M=\dfrac{N_c h\pi r\mu A_{PM}a_4}{2l_m^{\,2}} \\ K_t=\dfrac{N_c h\pi r\mu A_{PM}a_1}{l_m} \end{cases} \quad (14)$$

B. General Model

In order to achieve fault-tolerant operation, a general fault-tolerant mathematical model of PMBSM is necessary. In this mathematical model, the currents in five phases are independent with each other.

If we caculate the flux dentisy by using (3) directly and according to the Maxwell force formula, the forces will be expressed as:

$$\begin{cases} F_{Mx}=\dfrac{rh}{2\mu_0}\sum_{i=1}^{10}\int_{\frac{i-1}{5}\pi}^{\frac{i}{5}\pi}(F_{MMF}G_\mu+B_{PM})^2\cos\alpha\,d\alpha \\ F_{My}=\dfrac{rh}{2\mu_0}\sum_{i=1}^{10}\int_{\frac{i-1}{5}\pi}^{\frac{i}{5}\pi}(F_{MMF}G_\mu+B_{PM})^2\sin\alpha\,d\alpha \end{cases} \quad (15)$$

Simplified (15) and Maxwell forces are as the following:

$$\begin{cases} F_{Mx}=k_M\{[0.588(i_2-i_5)-0.951(i_3-i_4)]\sin\theta_r+[i_1-0.809(i_2+i_5)+0.309(i_3-i_4)]\cos\theta_r\} \\ F_{My}=k_M\{[0.588(i_2-i_5)-0.951(i_3-i_4)]\cos\theta_r+[-i_1+0.809(i_2+i_5)-0.309(i_3+i_4)]\sin\theta_r\} \end{cases} \quad (16)$$

Where $k_M=\dfrac{\sqrt{5}N_c hr\mu_0 A_{PM}}{8l_m^{\,2}}$. The torque will also be obtained in a similar method as (9). At last, the torque model is expressed as:

$$T=k_t\{[0.951(i_2-i_5)+0.588(i_3-i_4)]\cos\theta_r+[-i_1-0.309(i_2+i_5)+0.809(i_3+i_4)]\sin\theta_r\} \quad (17)$$

Where $k_t=\dfrac{N_c hr\mu_0 A_{PM}}{l_m}$. In fact, equtation (16) and (17) can be simplified in the maxtrix form as

$$[P]=[M]\cdot[i] \quad (18)$$

Where $[P]=[F_{Mx}\ F_{My}\ T]^{\mathrm{T}}$,$[i]=[i_1\ i_2\ i_3\ i_4\ i_5]^{\mathrm{T}}$ and $[M]$ is as the following:

$$\begin{bmatrix} k_M\cos\theta_r & k_M\cos(\theta_r+\frac{6\pi}{5}) & k_M\cos(\theta_r+\frac{2\pi}{5}) & k_M\cos(\theta_r+\frac{8\pi}{5}) & k_M\cos(\theta_r+\frac{4\pi}{5}) \\ k_M\sin(\theta_r+\pi) & k_M\sin(\theta_r+\frac{\pi}{5}) & k_M\sin(\theta_r-\frac{3\pi}{5}) & k_M\sin(\theta_r+\frac{3\pi}{5}) & k_M\sin(\theta_r-\frac{\pi}{5}) \\ k_t\sin(\theta_r+\pi) & k_t\sin(\theta_r+\frac{3\pi}{5}) & k_t\sin(\theta_r+\frac{\pi}{5}) & k_t\sin(\theta_r-\frac{\pi}{5}) & k_t\sin(\theta_r-\frac{3\pi}{5}) \end{bmatrix} \quad (19)$$

III. VERIFICATION BY FINITE ELEMENT ANALYSIS

In this section, finite element analysis (FEA) is done for detailed verification of the model. Table I shows the motor parameters in Ansoft.

TABLE I. PAPAMETEROF THE MOTOR

	Parameter	Value
r	Rotor diameter	16mm
W	Number of winding turns	12
h	Axial rotor length	10mm
l_m	Equivalent length of air gap	2.9mm
l_{PM}	Thickness of the PM	1.8mm

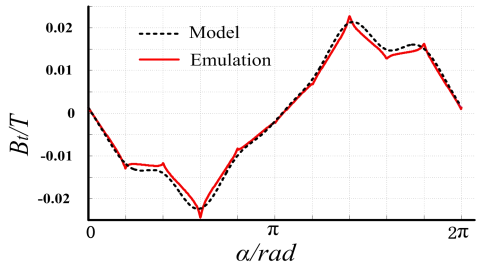

Figure 5. Comparison of the theoretical and emulational torque flux density when θ_t=56°

Fig.5 and Fig.6 show the comparison of torque air gap flux density and levitation air gap flux density between analytical result and finite element result, which are both only caused by stator currents. It can be seen from these two figures that the analytical results and finite element results agree well.

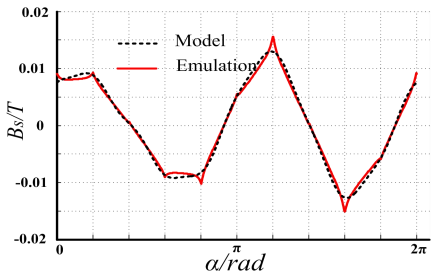

Figure 6. Comparison of the theoretical and emulational levitation flux density when θ_s=275°

To verify the exactitude of levitation, we do a preliminary validation in Ansoft. The rotor is kept still. Rotate the magnetic field produced by levitation currents and observe the levitation forces. The curves of them are shown in Fig.7.

In Fig.7, it is obvious that the levitation forces in FEA are much larger than the theoretical value. The error is high up to 30%. We have to conjecture that another kind of force may increase the levitation force.

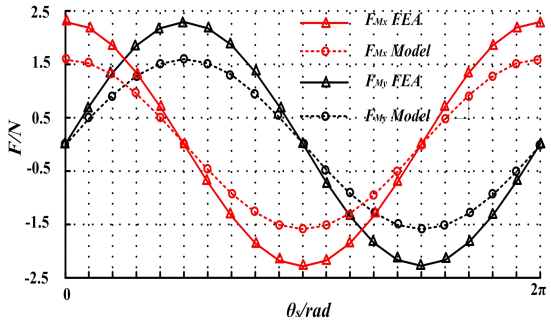

Figure 7. Comparison of the radial forces in Ansoft and the Maxwell forces

As we all know, there are two kinds of electromagnetic forces exsiting in the motor. One is the Maxwell force and its main effect is producing the levitation force as we deduced in last section. The other is Lorentz force, whose main effect is exerting a torque. In traditonal slice motor with stator teeth, the Lorentz force only has a minor effect on the levitation force. Usually, the Lorentz component in levitation force is small enough to be ignored. But it is still need to be verified whether the Lorentz force will cause such a big error in this slotless structure.

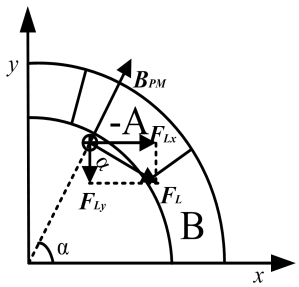

Figure 8. Schematic diagram of the Lorentz force on the stator wires

As shown in Fig.8, to analyse the Lorentz force, we take a part of the wires for infinitesimal analysis. The number of the wires is $N_c d\alpha$. According to the Lorentz fomula, the Lorentz force acting on these wires is:

$$dF_L = BIhA_f d\alpha = B_{PM}\cos(\alpha-\theta_r)IhN_c d\alpha \tag{20}$$

Where B_{PM} is the amplitude of flux density produced by PM, I is the current in the wires. The force is always along the tangent direction of the circumference. Then we decompose the force to x and y directions as (21):

$$\begin{cases} dF_{Lx} = B_{PM}IhN_c\cos(\alpha-\theta_r)\sin\alpha d\alpha \\ dF_{Ly} = -B_{PM}IhN_c\cos(\alpha-\theta_r)\cos\alpha d\alpha \end{cases} \tag{21}$$

Integrate the force F_{Lx} under each coil like fomula (22):

$$\begin{aligned} F_{Lx} &= \int_0^{2\pi} B_{PM}IhN_c\cos(\alpha-\theta_r)\sin\alpha d\alpha \\ &= B_{PM}hN_c\sum_{k=1}^{5}\Big[\int_{(2k-4)\pi/5}^{(2k-3)\pi/5} i_k\cos(\alpha-\theta_r)\sin\alpha d\alpha \\ &\quad + \int_{(2k-1)\pi/5}^{2k\pi/5} -i_k\cos(\alpha-\theta_r)\sin\alpha d\alpha\Big] \end{aligned} \tag{22}$$

If the constraint relationship of the currents (1) is put into (22) and the force in x direction is as the following:

$$F_{Lx} = -\frac{5\sqrt{5}}{8}N_c B_{PM}hI_s\cos(\theta_s-\theta_r) \tag{23}$$

Caculate the F_{Ly} in the same method and the result will be achieved:

$$F_{Ly} = \frac{5\sqrt{5}}{8}N_c A_{PM}\frac{\mu_0}{l_m}hI_s\sin(\theta_r-\theta_s) \tag{24}$$

Considering the force acting on the rotor is the opposite reaction of the force on the wires, we rewrite the forces as (25):

$$\begin{cases} F_{Lx} = K_L\cos(\theta_s-\theta_r)I_s \\ F_{Ly} = K_L\sin(\theta_s-\theta_r)I_s \end{cases} \tag{25}$$

Where $K_L = \frac{5\sqrt{5}N_c A_{PM}\mu_0 h}{8l_m}$. Compare the Lorentz forces (25) with Maxwell forces and we'll find that these two forces have no differences in the form except the coefficient. Hence, the radial levitaiton forces in five-phase constraint model, which is made up of Maxwell component and Lorentz component, are corrected as (19):

$$\begin{cases} F_x = (K_L+K_M)\cos(\theta_s-\theta_r)I_s = K_s\cos(\theta_s-\theta_r)I_s \\ F_y = (K_L+K_M)\sin(\theta_s-\theta_r)I_s = K_s\cos(\theta_s-\theta_r)I_s \end{cases} \tag{26}$$

Where $K_s=K_L+K_M$. If the current relationship is not put into (22), we'll get the general form of the Lonrentz forces as :

$$\begin{cases} F_{Lx} = k_L\{[0.588(i_2-i_5)-0.951(i_3-i_4)]\sin\theta_r + \\ \qquad [i_1-0.809(i_2+i_5)+0.309(i_3-i_4)]\cos\theta_r\} \\ F_{Ly} = k_L\{[0.588(i_2-i_5)-0.951(i_3-i_4)]\cos\theta_r + \\ \qquad [-i_1+0.809(i_2+i_5)-0.309(i_3+i_4)]\sin\theta_r\} \end{cases} \tag{27}$$

Where $k_L = \frac{\sqrt{5}N_c h\mu_0 A_{PM}}{4l_m}$. Similarly, correct the general model as

$$\begin{bmatrix} F_x \\ F_y \\ T \end{bmatrix} = \begin{bmatrix} k_s\cos(\theta_r) & k_s\cos(\theta_r+\frac{6\pi}{5}) & k_s\cos(\theta_r+\frac{2\pi}{5}) & k_s\cos(\theta_r+\frac{8\pi}{5}) & k_s\cos(\theta_r+\frac{4\pi}{5}) \\ k_s\sin(\theta_r+\pi) & k_s\sin(\theta_r+\frac{\pi}{5}) & k_s\sin(\theta_r-\frac{3\pi}{5}) & k_s\sin(\theta_r+\frac{3\pi}{5}) & k_s\sin(\theta_r-\frac{\pi}{5}) \\ k_t\sin(\theta_r+\pi) & k_t\sin(\theta_r+\frac{3\pi}{5}) & k_t\sin(\theta_r+\frac{\pi}{5}) & k_t\sin(\theta_r-\frac{\pi}{5}) & k_t\sin(\theta_r-\frac{3\pi}{5}) \end{bmatrix}\begin{bmatrix} i_1 \\ i_2 \\ i_3 \\ i_4 \\ i_5 \end{bmatrix} \tag{28}$$

Where $k_s=k_L+k_M$.

Replot the levitation forces as Fig.9. This time the force in model is greater than that in FEA on the contray, but their values are very close and the error is only about 5%. If the exsitence of flux leakage, magnetic saturation magnetic and motive force drop in iron are taken into account, this result is relatively reasonable.

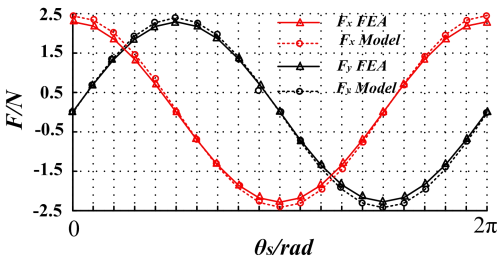

Figure 9. Comparison of the levitation forces

Next, levitation force and torque characteristics will be prensented. Here, we set I_t=3A, I_s=2A, $\theta_s=\theta_r+45°$,$\theta_t=\theta_r+90°$ and change the rotor angle θ_r from 0 to 2π. In Fig.10, it can be seen that the torque in FEA maintains stable, though a small error, which is no more than 4%, is observed. The causes of it are no other than the assumption *a* and *c*. These two assumptions both made the value of the flux density in our calculation greater.

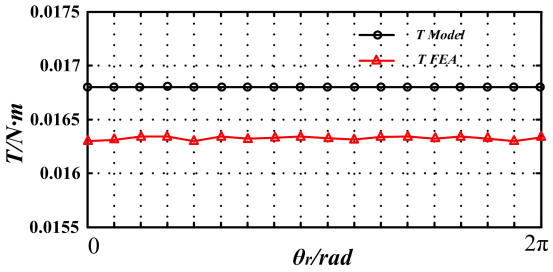

Figure 10. Curve of the torque changing with θ_r

Fig.11 illustrates that the levitation force is stable basically though there is pulsation in it. From (10) and (11), we can easily know the pulsation is caused by the first term. In addition, the force in *x* and *y* direction should be equal theoretically when $\theta_s=\theta_r+45°$, but these two values in FEA deviate a little. This is the effect of the second term, which is relevant to the torque current. Although these two problems affect the accuracy of the model, they are not so obvious and still in the acceptable range when the current is not so heavy.

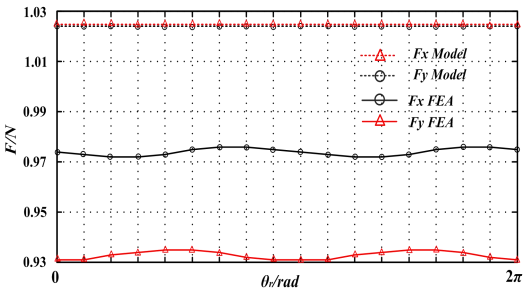

Figure 11 Curve of the levitation forces changing with θ_r

If we keep θ_r=0°, $\theta_s=\theta_r+45°$, $\theta_t=\theta_r+90°$ and change the value of I_s and I_t, curves of torque and levitation forces changing with amplitude of currents will be achieved as Fig.12 and Fig.13

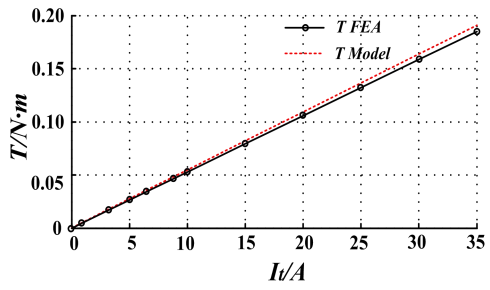

Figure 12. Curve of torque changing with I_t

It can be seen that there is high linearity between torque and I_t, though the torque in FEA is sightly less than that in theory, the error is about just 3%.

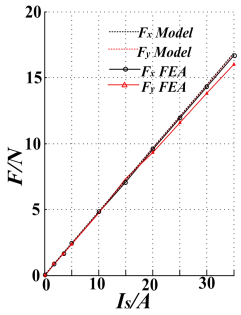

Figure 13. Curve of torque changing with I_s when I_t=0

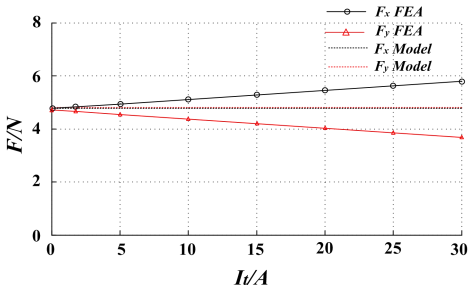

Figure 14. Curve of the levitation forces changing with I_t when I_s=10A

Fig.13 shows that the levitation forces in FEA has a linear relationship with I_s when there are no torque current component. But from Fig(14), it can be seen that with the increase of I_t, the levitation forces are becoming skewed. That's the result of the coupling between levitation force and I_t . From (10) and (11), we can kown that the effect of coupling will be obvious when I_t is large enough. Thus, in actual situation, I_t will affect the peformance of radial disposition control in a certain extent.

In order to make model more precise, two compensation coefficients σ_t and σ_s are introduced to fix the expressions. In five-phase constraint model, K_s and K_t are updated as:

$$\begin{cases} K_s = \sigma_s (K_L + K_M) \\ K_t = \sigma_t \dfrac{N_c hr \mu_0 A_{PM} a_1}{l_m} \end{cases} \tag{29}$$

Similarly, in the general model k_s and k_t are updated as :

$$\begin{cases} k_s = \sigma_s (k_L + k_M) \\ k_t = \sigma_t \dfrac{N_c hr \mu_0 A_{PM}}{l_m} \end{cases} \tag{30}$$

Where σt is 0.97 and σs is 0.95.

IV. CONCLUSION

Five-phase constraint model and general model of the slotless PMBSM are deduced in this paper. The first model is relatively simple in the form, though it is not as applicable as the general one. The general model is the theoretical basis of the research on fault-tolerant capability. Because the flux density in the air gap is the key to gain the torque and the levitation force, a verification about it is done. After that, levitaiton force and torque characteristics are investigated by FEA. The result shows both of the models are accurate enough to describe the slotless PMBSM in the case that current is not too heavy.

REFERENCES

[1] Steinert, Daniel, Thomas Nussbaumer, and Johann W. Kolar. "Concept of a 150 krpm bearingless slotless disc drive with combined windings." Electric Machines & Drives Conference (IEMDC), 2013 IEEE International. IEEE, 2013.

[2] H. Mitterhofer, D. Andessner, and W. Amrhein, “Analytical and experimental loss examination of a high speed bearingless drive,” in Proc. International Symposium on Power Electronics Electrical DrivesAutomation and Motion, 2012.

[3] Hubert Mitterhofer, Wolfgang Gruber, and Wolfgang Amrhein, “ On the High Speed Capacity of Bearingless Drives,” in IEEE Transactions onIndustrial Electronics, 2013.

[4] Zhu, Huangqiu, et al. "Mathematical model and control technology of bearingless PMSM." Control and Decision Conference (CCDC), 2010 Chinese. IEEE, 2010.

[5] Xiao-lin, Wang, et al. "Current-controlled multiphase slice permanent magnetic bearingless motors with open-circuited phases: Fault-tolerant controllability and its verification." Industrial Electronics, IEEE Transactions on 59.5 (2012): 2059-2072.

[6] Wang, X. L., et al. "Fault-tolerant control of multi-phase permanent magnetic bearingless motors." Electrical Machines (ICEM), 2010 XIX International Conference on. IEEE, 2010.